PAPER

Check for updates

Unraveling the origin of the "Turn-On" effect of Al-MIL-53-NO$_2$ during H$_2$S detection†

Zan Zhu, Xiang He and Wei-Ning Wang ⓘD *

Nitro-functionalized metal–organic frameworks (MOFs), such as Al-MIL-53-NO$_2$, have been widely used in quantitative hydrogen sulfide (H$_2$S) detection based on the "turn-on" effect, where fluorescence enhancements were observed upon contact with H$_2$S. This was believed to be caused by the fact that the electron-withdrawing –NO$_2$ groups in the initial non-luminescent MOFs were reduced to electron-donating –NH$_2$ groups in the sensing process. However, since most H$_2$S detection is conducted in a suspension system consisting of MOFs and solvents, it is still unclear whether these –NH$_2$ groups are on MOFs or in the liquid. Using Al-MIL-53-NO$_2$ as a model MOF, this work aims to answer this question. Specifically, the supernatant and undissolved particles separated from the Al-MIL-53-NO$_2$ suspensions after being exposed to H$_2$S were analyzed systematically. The results showed that it is the free BDC-NH$_2$ (2-aminobenzene-1,4-dicarboxylic acid) in the solution rather than the formation of Al-MIL-53-NH$_2$ that really caused the fluorescence enhancement. In particular, the formed BDC-NH$_2$ was reduced from the shedded BDC-NO$_2$ (2-nitrobenzene-1,4-dicarboxylic acid) during the decomposition of Al-MIL-53-NO$_2$, which was attacked by OH$^-$ in the NaHS solution. We anticipate that this work will offer new ways of tracing fluorophores for MOF-based sensing applications in aqueous systems.

1. Introduction

Hydrogen sulfide (H$_2$S), known by its characteristic odor of rotten eggs, has been receiving considerable attention because it is highly associated with the physiological and pathological processes in biological systems.[1,2] Abnormal levels of H$_2$S have been identified to be related to many complex diseases such as Alzheimer's disease,[3] diabetes,[4] Down's syndrome,[5] arterial and pulmonary hypertension,[6] Parkinson's disease,[7] and periodontal disease,[8] which makes H$_2$S detection significant in disease prevention and diagnosis. Various methods towards H$_2$S sensing have been proposed, including semiconductor-based electrochemical tests,[9] direct gas chromatography measurements,[8] and piezoelectric transducer detection.[10] However, the development of these methods is hampered by expensive instruments, complexity in sample preparation, and complicated operating procedures. The fluorescence-based detection method has grown rapidly in recent years because of its high selectivity and sensitivity, short response time, simplicity of operation, and easy observation

in real-time imaging.[11,12] Up till now, plenty of fluorescent materials have been designed and used for H$_2$S sensing.[13–15]

Among these fluorescent materials, metal–organic frameworks (MOFs), a class of porous crystalline materials composed of bridged organic linkers and centered metal ions/clusters,[16] are interesting candidates because the great abundance of functional ligands and metals endow MOFs with very promising physical and chemical properties.[17–20] Several luminescent MOFs have been used for H$_2$S detection in aqueous or real physiological systems.[21–37] Among these explored mechanisms of H$_2$S sensing, the "turn-on" effect is the most popular one, where the original non-luminescent MOFs in the "turn-off" state are activated and enhanced upon being exposed to H$_2$S. Nitro-functionalized MOFs have been proven to be effective probes for H$_2$S detection based on the "turn-on" effect.[22,23,35] Specifically, the nitro groups (–NO$_2$) in nitro-functionalized MOFs decrease the electron density of the aromatic ring because of the unpaired electrons on nitrogen, which makes MOFs emit very weak fluorescence and stay in the "turn-off" state. After being treated by H$_2$S, electron-donating –NH$_2$ groups are obtained and the "turn-on" fluorescence signal is captured.

Based on this mechanism, Zr-UiO-66-NO$_2$ was first synthesized by Ghosh *et al.* to realize the "turn-on" response towards 0.0–4.0 mM H$_2$S through the transformation of Zr-UiO-66-NO$_2$ to Zr-UiO-66-NH$_2$.[21] Later on, Biswas *et al.* reported Ce-UiO-66-NO$_2$,[23] DUT-52-(NO$_2$)$_2$,[26] and Zr-UiO-66-

Department of Mechanical and Nuclear Engineering, Virginia Commonwealth University, Richmond, Virginia 23219, USA. E-mail: wnwang@vcu.edu; Fax: +1 804 827 7030; Tel: +1 804 827 4306
† Electronic supplementary information (ESI) available. See DOI: 10.1039/c9ce01595g

$(NO_2)_2$ (ref. 32) for quantitative H_2S detection in physiological systems and living cells. The lowest detection limit at 92.31×10^{-9} M was recently reported by Qian *et al.* using polymer mixed-matrix membranes (MMM) developed by the combination of Al-MIL-53-NO_2 nanoparticles and PVDF (polyvinylidene fluoride).[35] Among all these nitro-functionalized MOF compounds, linear relationships were obtained in the different ranges of H_2S concentrations with the fluorescence intensity, which can be applied for real quantitative H_2S sensing.

As most of these "turn-on" assays have been conducted in a suspension system, where the solid-state nitro-functionalized MOFs were dispersed in NaHS/Na_2S solutions, the fluorescence obtained was actually attributed to the combined effects of real fluorophores and non-luminescent particles in the suspension. Even though the researchers ascribed the fluorescence enhancement in the suspension to the formation of NH_2-functionalized MOFs, the direct evidence of $-NH_2$ existence within the MOFs after H_2S treatment is still lacking. In addition, misinterpretation of fluorescent signals may also arise for the following reasons: 1. the precipitation of undissolved particles in the suspension will change the pathway of excitation radiation, which further leads to fluctuations in the fluorescence intensity; 2. the irradiation could be absorbed by the non-luminous undissolved particles in the suspensions, which decreases the effective light for absorption by real fluorophores. This phenomenon is called inner-filter effect and the existence of high concentrations of non-luminous undissolved particles can reduce the fluorescence intensity; 3. except for absorption, the irradiation light is also scattered in all directions from the small molecules in the suspensions. In a case of a suspension with a small Stokes shift, the broad scattering peak near the excitation wavelength sometimes may overlap with the emission peak, which makes the fluorescence intensity from fluorophores difficult to separate. Therefore, it is sometimes difficult to identify the real fluorophores in such a complex suspension system.

To further explore the mechanism of the "turn-on" effect, Al-MIL-53-NO_2 was utilized in this study to react with H_2S in an aqueous system. Furthermore, the supernatant and the undissolved particles were isolated for the first time to locate the possibly formed $-NH_2$ groups. Meanwhile, the effect of the undissolved MOF particles on the fluorescence intensity in the sensing application was also analyzed. Interestingly, after being treated with H_2S (0.1–1.0 mM), the undissolved nanoparticles that remained in the suspension were proved to be Al-MIL-53-NO_2 rather than Al-MIL-53-NH_2 and no $-NH_2$ groups were formed at the surface of the residual solids, which made no contribution to fluorescence enhancement. The fluorescence "turn-on" effect was actually caused by the free BDC-NH_2 in the solution, which was reduced from BDC-NO_2 in the collapse of Al-MIL-53-NO_2 when exposed to H_2S. With the existence of the fluorophore BDC-NH_2 in the aqueous system, both the supernatant (limit of detection, LOD = 69.7 μM) and suspension (*i.e.*, Al-MIL-53-NO_2 particles were

dispersed evenly in aqueous solutions of NaHS by ultrasonication) (LOD = 69.3 μM) can be used to realize quantitative H_2S sensing within 0–0.7 mM H_2S. The result of this work unravels the origin of the "turn-on" effect of Al-MIL-53-NO_2 in H_2S sensing and explores new ways (separation of suspension into supernatant and undissolved residues) of fluorophore tracing in MOF-based detection.

2. Materials and methods

2.1 Chemicals

Sodium hydrosulfide hydrate (NaHS·xH_2O, ~70%), 2-nitrobenzene-1,4-dicarboxylic acid ($C_8H_5NO_6$, BDC-NO_2, ≥99%), 2-aminobenzene-1,4-dicarboxylic acid ($C_8H_7NO_4$, BDC-NH_2, ≥99%), and aluminum chloride hexahydrate ($AlCl_3$ ·$6H_2O$, ≥99%) were obtained from Sigma Aldrich. *N*-Dimethylformamide ($HCON(CH_3)_2$, DMF) was purchased from VWR Corporation. Ethanol (C_2H_5OH, 190 proof) was obtained from Gold Shield. Deionized (DI) water was used to prepare the solutions. All chemicals were used without further purification.

2.2 Synthesis of Al-MIL-53-NO_2 and Al-MIL-53-NH_2

2.2.1 Al-MIL-53-NO_2. Al-MIL-53-NO_2 nanoparticles were synthesized according to a previous report.[35] Typically, BDC-NO_2 (42.2 mg, 0.2 mmol) was dissolved in 10 mL DMF by sonication for 1 minute. Then, $AlCl_3$·$6H_2O$ (48.3 mg, 0.2 mmol) with the above solution was transferred into a 25 mL Teflon lined steel autoclave and heated at 180 °C for 12 hours. The obtained yellow particles were separated by centrifugation at 10 000 rpm for 10 minutes and washed with 15 mL DMF and 15 mL ethanol three times to remove unreacted chloride species and BDC-NO_2. Finally, the collected particles were dried in air at 200 °C for 6 hours to completely remove the attached DMF molecules.

2.2.2 Al-MIL-53-NH_2. Al-MIL-53-NH_2 was prepared based on a reported synthetic procedure.[38] $AlCl_3$·$6H_2O$ (1.45 g, 6.0 mM) and 2-aminobenzene-1,4-dicarboxylic acid (BDC-NH_2) (1.1 g, 6.0 mM) were mixed in 30 mL DMF and then kept in a 100 mL Teflon lined steel autoclave at 150 °C for 5 hours. After being cooled to room temperature, the obtained yellow particles were washed with 15 mL DMF and 15 mL ethanol three times. The as-synthesized Al-MIL-53-NH_2 was activated in 60 mL DMF solution at 155 °C for 24 hours and then heated in air at 155 °C for 24 hours.

2.3 Materials' characterization

The morphologies of the samples were analyzed using a scanning electron microscope (SEM) with energy dispersive X-ray (EDX) spectroscopy (Su-70, Hitachi). The structure and crystallinity of Al-MIL-53-NO_2 were determined by powder X-ray diffraction (PXRD) (PANalytical X'Pert Pro MPD). The analysis of vibrations of the functional groups was carried out with a Fourier transform infrared (FT-IR) spectrometer (Nicolet iS50, Thermo Scientific). The photoluminescence properties of the

samples were characterized by a fluorospectrometer (PTI QuantaMaster-400). X-ray photoelectron spectroscopic (XPS) measurement was conducted with a Thermo Scientific ESCALAB 250 to investigate the chemical state of the element on the surface of Al-MIL-53-NO$_2$. The pore size and surface area of Al-MIL-53-NO$_2$ were measured by using Autosorb iQ (Quantachrome Instruments).

2.4 H$_2$S fluorescence sensing measurements

NaHS was used as the H$_2$S source and dissolved in DI water to form a transparent solution.[23,25,35] In this paper, "H$_2$S treated" or "H$_2$S treatment" means that Al-MIL-53-NO$_2$ is suspended in NaHS solution with a specific concentration. In a typical experiment, 1.5 mg Al-MIL-53-NO$_2$ was suspended into the cuvette containing 3.0 mL NaHS solution with various concentrations (0.0–5.0 mM) for 2 hours before centrifugation. The corresponding supernatant and the suspended undissolved particles were separated by centrifugation at 12 000 rpm for 10 minutes. The re-collected particles were washed with water three times and re-dispersed into 3.0 mL DI water for further photoluminescence measurement. For all the fluorescence measurements, the excitation wavelength (λ_{ex}) was 339 nm and the emission spectra were recorded in the range of 380–580 nm. Both the emission and excitation slits were set to be 2 nm.

3. Results and discussion

3.1 Characterization of Al-MIL-53-NO$_2$

The crystallinity and structure of Al-MIL-53-NO$_2$ were determined by PXRD. As shown in Fig. 1a, all the peaks are consistent with those as reported in the previous references, where Al-MIL-53-NO$_2$ has a monoclinic crystal structure.[35,39,40] The main peak was located at ~8.5°, which is ascribed to the (100) plane.[39] The crystals and morphologies were also characterized by scanning electron microscopy (SEM). It was found that the Al-MIL-53-NO$_2$ powders are composed of irregular nanoparticles with sizes ranging from 20 nm to 300 nm (Fig. 1b), which is also similar to that reported previously.[35] In addition to the crystallinity and morphology, the vibrational analysis of the surface functional groups was directly carried out by FT-IR. The absorption peak at 1542 cm^{-1} (Fig. 1c) originated from the N=O stretching vibration of the nitro groups attached to the coordinated ligands, which demonstrated the successful incorporation of –NO$_2$ group into the MOF crystals.[26] The strong absorption bands at 1421 cm^{-1} and 1619 cm^{-1} are attributed to the symmetric and asymmetric –CO$_2$ stretching vibrations from the coordinated BDC-NO$_2$ linkers, respectively. It should be noted that the small peak at 3662 cm^{-1} is ascribed to the μ_2-OH group.[39] The porosity of Al-MIL-53-NO$_2$ was further confirmed by the N$_2$ sorption measurements at 77 K. As shown in Fig. 1d, the rapid increase in the low relative pressure regions demonstrated the existence of micropores in
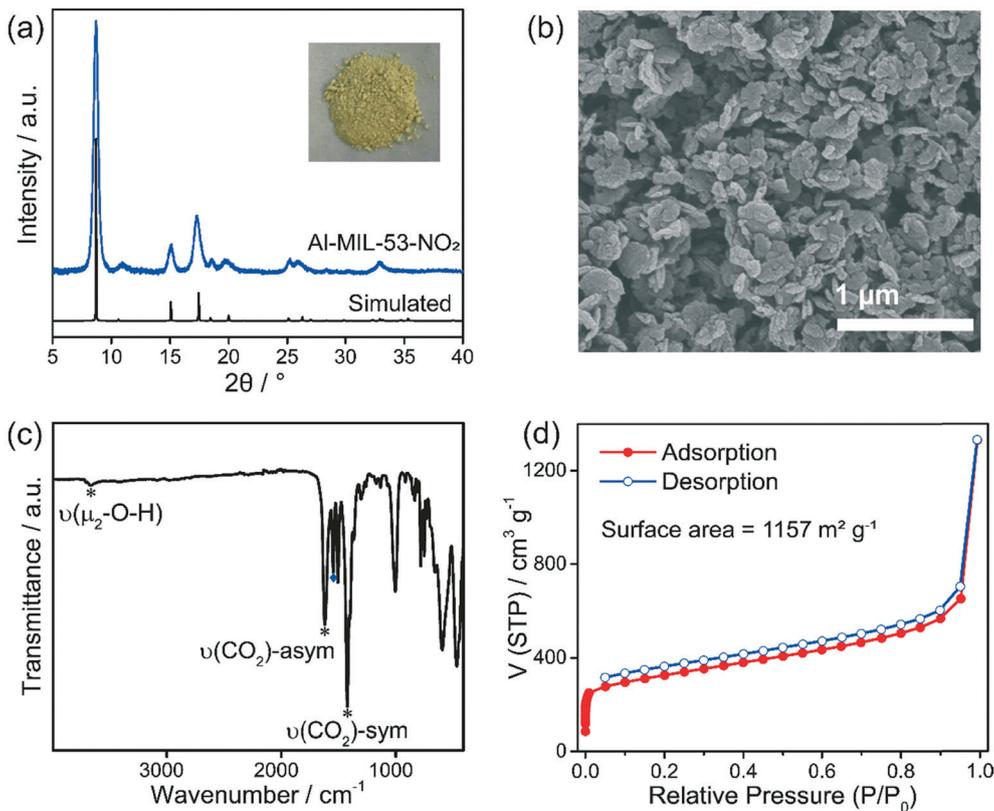

Fig. 1 (a) PXRD patterns and digital image (inset), (b) SEM image, (c) FT-IR spectrum, and (d) gas sorption isotherms of the Al-MIL-53-NO$_2$ nanoparticles.

Al-MIL-53-NO$_2$. The surface area of Al-MIL-53-NO$_2$ based on the Brunauer–Emmett–Teller (BET) theory was calculated to be 1157 m^2 g^{-1}, which provides a large number of active sites to interact with H$_2$S in the sensing process (detailed BET surface area calculation and plots are shown in ESI† S1 and Fig. S1).[41–44] Overall, the above results indicated that Al-MIL-53-NO$_2$ was synthesized successfully.

3.2 H$_2$S sensing performance

The detection capability of Al-MIL-53-NO$_2$ for H$_2$S was investigated by performing fluorescence "turn-on" experiment in the aqueous suspension system. NaHS was used as the source of H$_2$S in this study.[25,35] Owing to the existence of electron-withdrawing nitro groups in the coordinated BDC-NO$_2$ ligand, Al-MIL-53-NO$_2$ is non-luminous and remains in the fluorescence "turn-off" state.[35] Once exposed to H$_2$S, –NO$_2$ is reduced to the electron-donating –NH$_2$ groups and fluorescence enhancement was observed based on the following reaction:
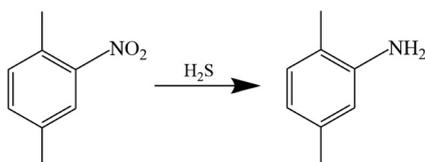
For H$_2$S sensing quantification, 1.5 mg Al-MIL-53-NO$_2$ was suspended in 3 mL DI water with various NaHS concentrations from 0.0 mM to 5.0 mM. To ensure the complete conversion of –NO$_2$ to –NH$_2$ in the sensing process, the suspension was kept in a sealed glass vial for 2 hours and then shaken to form a uniform suspension for photoluminescence measurement. The excitation wavelength was determined at 339 nm by scanning 1.0 mM H$_2$S treated Al-MIL-53-NO$_2$ suspension from 380 nm to 580 nm with the maximum emission peak located at 450 nm, as shown in Fig. S2.† All the fluorescence emission spectra were recorded in the range from 380 nm to 550 nm at the excitation wavelength of 339 nm in this study. It is found that H$_2$S showed a significant "turn-on" response to the Al-MIL-53-NO$_2$ suspensions (Fig. 2a–c). An excellent linear correlation (R^2 = 0.98498) was obtained between the fluorescence intensities and H$_2$S concentrations within 0.7 mM (Fig. 2d). Moreover, the limit of detection (LOD) was calculated to be 69.3 μM (detailed LOD calculations are shown in ESI† S2), which indicated that Al-MIL-53-NO$_2$ can be used for the quantitative detection of H$_2$S in the aqueous suspension system. It is noteworthy that the fluorescence intensity was vastly enhanced when the H$_2$S concentration was larger than 1.0 mM and tended to be constant within the range from 2.0 mM to 5.0 mM. The possible mechanisms for such significant "turn-on" fluorescence increment will be discussed in the next section.
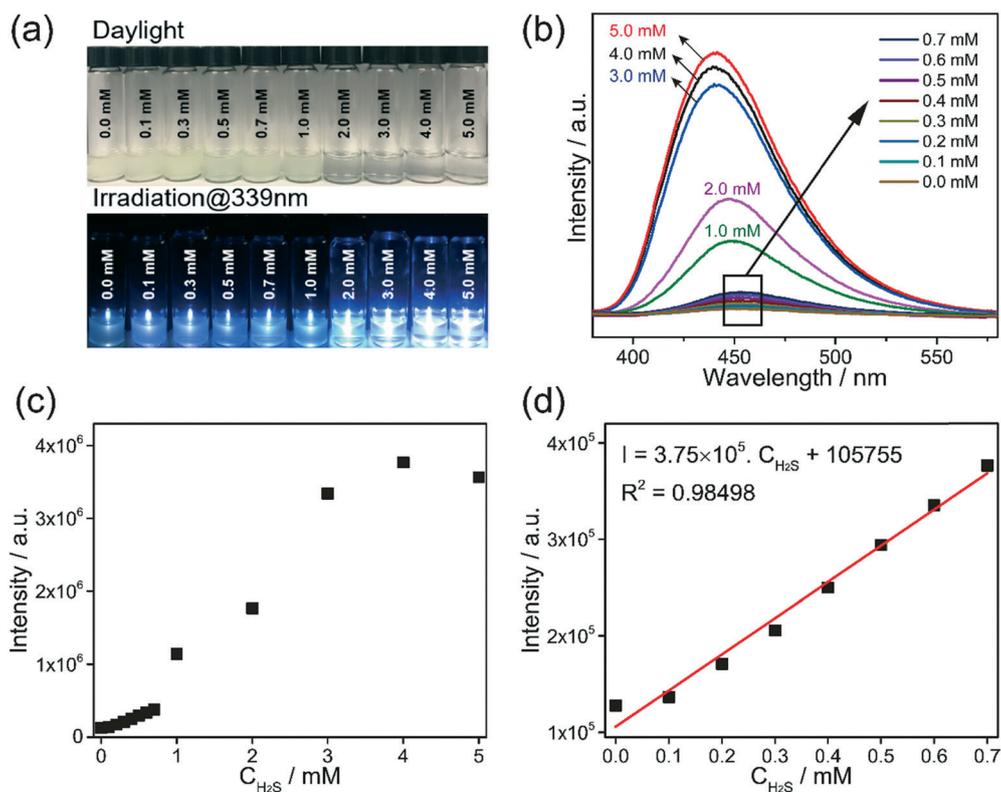

Fig. 2 (a) Digital images of Al-MIL-53-NO$_2$ suspensions with various NaHS concentrations under visible light (up) and UV light (339 nm, down); (b) emission spectra of Al-MIL-53-NO$_2$ suspensions with various NaHS concentrations (excitation wavelength: 339 nm); (c and d) emission intensity *versus* NaHS concentration.

3.3 Exploration of the "Turn-On" effect

Most studies ascribe the "turn-on" effect to the conversion of –NO$_2$ to –NH$_2$ groups by "MOF transformation" and fluorescence signals of MOFs in the suspension were used for quantitative H$_2$S detection. Few researchers separated the undissolved particles to give direct evidence of –NH$_2$ groups on the surface of MOF after exposure to H$_2$S. In order to determine whether luminescence enhancement comes from the –NH$_2$ groups in MOF or the free ones in the solution, the suspensions were centrifuged at 12 000 rpm for 10 minutes to separate the undissolved particles and supernatant for further analysis (see Scheme 1). The exploration of the "Turn-On" effect was carried out through the analysis of both undissolved nanoparticles (section 3.3.1) and supernatant (section 3.3.2).

3.3.1 Analysis of undissolved nanoparticles. The undissolved nanoparticles separated from the suspensions were washed with DI water three times and dried in air at 120 °C for two hours to remove the water molecules. The 0.5 mM and 1.0 mM H$_2$S treated Al-MIL-53-NO$_2$ were characterized by PXRD. The PXRD patterns matched well with the pristine Al-MIL-53-NO$_2$ nanoparticles and no apparent phase of the as-synthesized Al-MIL-53-NH$_2$ was observed (Fig. S3†). According to the Scherrer equation,

$$\tau = \frac{K\lambda}{\beta \cos \theta}$$

where τ is the mean size of the crystallite; K is the dimensionless shape factor ($K = 0.89$); λ is the X-ray wavelength ($\lambda = 1.5406$ Å); β is the line broadening at the maximum intensity or the so-called full width at half maximum (FWHM); θ is the Bragg angle, it was found that with H$_2$S concentration increased from 0.0 mM to 0.5 mM, and 1.0 mM, the FWHM of the peak at 8.5° becomes broader, and the corresponding calculated mean crystallite size within the (100) domain is reduced from 19.69 nm to 18.52 nm and 17.16 nm, respectively (Fig. 3(a–c)). The small shrinkage of the Al-MIL-NO$_2$ crystals could be caused by the original Al-MIL-53-NO$_2$ being degraded from outside to the core, where the peripheral bridged Al–O bonds were broken in the alkaline NaHS solution.[45] Similar morphologies of the recollected Al-MIL-53-NO$_2$

nanoparticles treated with 0.5 mM and 1.0 mM H$_2$S as compared to the pristine Al-MIL-53-NO$_2$ (Fig. 3(e–g)) confirmed that the residual Al-MIL-53-NO$_2$ nanoparticles kept the same shapes with the 1.0 mM H$_2$S treatment. When the H$_2$S concentration increased to 2.0 mM, the initial Al-MIL-53-NO$_2$ crystalline materials collapsed and an amorphous PXRD pattern was obtained (Fig. 3d). The large crystals disappeared, leaving much smaller amorphous particles, as shown in Fig. 3h. Interestingly, similar peak broadening phenomena were also observed in other nitro-functionalized MOFs (Zr-UiO-66-NO$_2$, Ce-UiO-66-NO$_2$, and Zr-UiO-66-(NO$_2$)$_2$) during H$_2$S detection,[22,23,32] which indicated that all these MOFs could be partially consumed and the particle sizes became smaller after being treated with H$_2$S. The particles with reduced crystal size and the released species into the solution could cause a dramatic change in the fluorescence intensity, which will be further discussed using Al-MIL-53-NO$_2$ in the next section (section 3.3.2).

The functional groups of the undissolved Al-MIL-53-NO$_2$ nanoparticles treated with 0.5 mM and 1.0 mM H$_2$S were analyzed by an FT-IR spectrometer. As shown in Fig. S4,† two major peaks were observed for Al-MIL-53-NH$_2$ at 3387 and 3499 cm^{-1}, corresponding to symmetric and asymmetric N–H stretching vibration, respectively. However, no apparent peaks were observed for the undissolved particles, which indicated that –NO$_2$ groups on undissolved Al-MIL-53-NO$_2$ nanoparticles were not reduced to –NH$_2$ groups after H$_2$S sensing.

Al-MIL-53-NO$_2$ before and after 1.0 mM H$_2$S treatment was further analyzed by X-ray photoelectron spectroscopy (XPS) (Fig. 4). For pristine Al-MIL-53-NO$_2$, the high-resolution spectrum of N 1s can be divided into two peaks located at 399.1 eV and 405.5 eV (Fig. 4a), which are attributed to N–C and –NO$_2$ groups within Al-MIL-53-NO$_2$, respectively.[46] After being exposed to 1.0 mM H$_2$S, no other peaks related to N 1s appeared (Fig. 4b) and the ratio of the peak area of N–O to C–N remained almost the same (before: 1.71 : 1; after 1.62 : 1), indicating that the undissolved Al-MIL-53-NO$_2$ nanoparticles in 1.0 mM H$_2$S solution shared similar surface chemical properties with the pristine unreacted Al-MIL-53-NO$_2$. Similar survey XPS pattern was also obtained for Al-MIL-53-NO$_2$ treated with 1.0 mM H$_2$S (Fig. S5†), where the peaks of binding energy at ∼532 eV, ∼405 eV, ∼285 eV, ∼119 eV, and ∼74 eV are ascribed to C 1s, N 1s, O 1s, Al 2s, and Al 2p, respectively. Moreover, the as-synthesized Al-MIL-53-NH$_2$ was used for comparison (Fig. S6†). The high-resolution N 1s spectrum of Al-MIL-53-NH$_2$ exhibits two peaks at 399.3 eV and 398.5 eV, which can be assigned to C–N bonds and NH$_2$ groups, respectively (Fig. S6†).[47] It is not surprising that this N 1s information related to Al-MIL-53-NH$_2$ cannot be observed in Fig. 4b since the 1.0 mM H$_2$S treated Al-MIL-53-NO$_2$ shared almost the same chemical properties with the unreacted one.

Additionally, the recollected Al-MIL-53-NO$_2$ nanoparticles after interaction with various concentrations of H$_2$S were resuspended in 3.0 mL DI water for further photoluminescence measurement. It turns out that all the
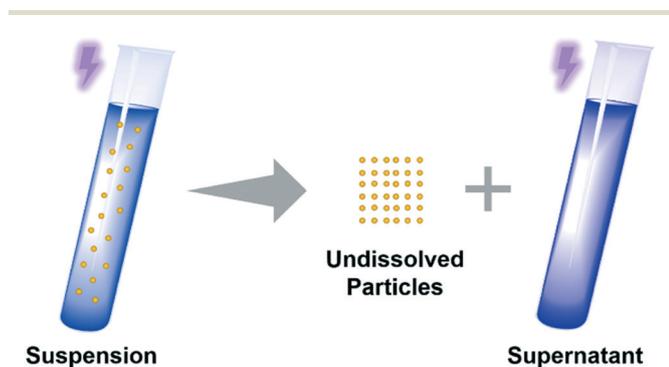
Scheme 1 Undissolved particles and supernatant were separated by centrifugation for further analysis.
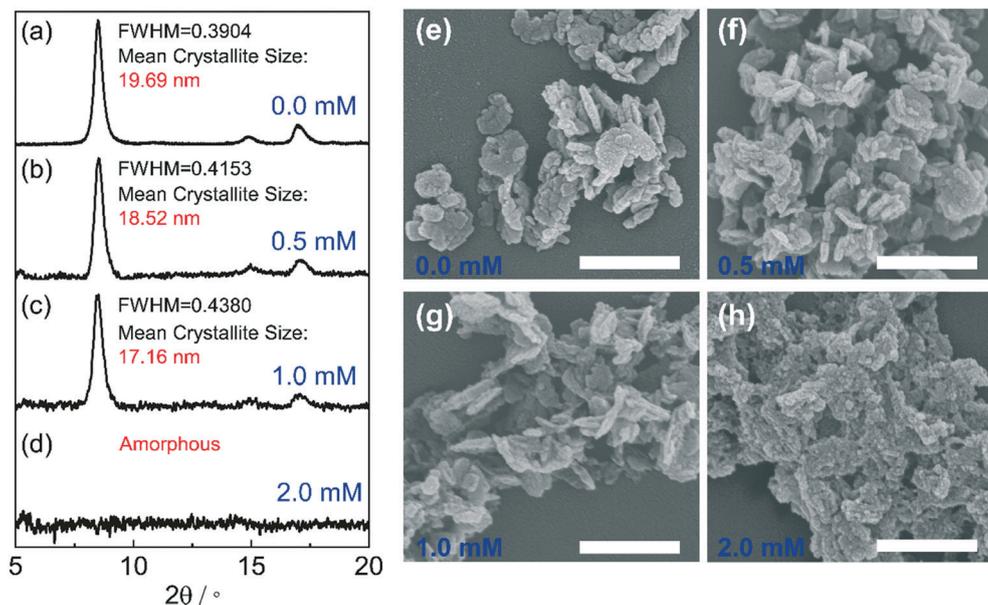
Fig. 3 PXRD patterns and SEM images of undissolved nanoparticles collected from Al-MIL-53-NO$_2$ suspensions with various NaHS concentrations: 0.0 mM (a and e), 0.5 mM (b and f), 1.0 mM (c and g), and 2.0 mM (d and h). The scale bar for (e–h) is 500 nm.
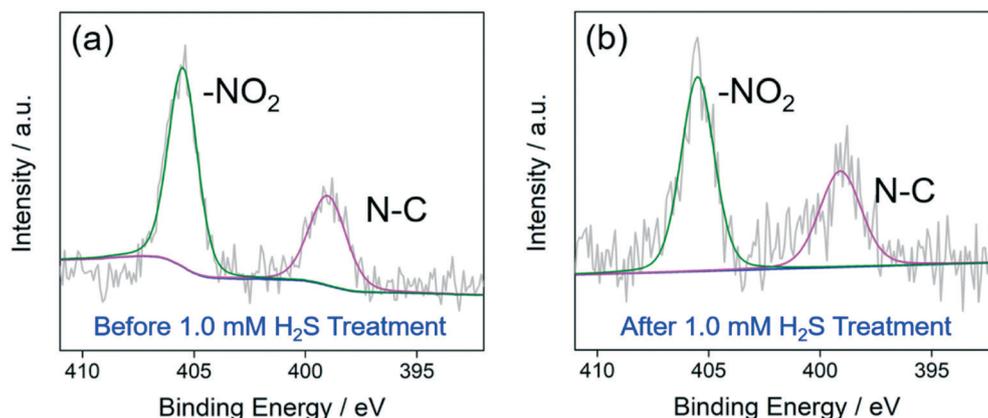

Fig. 4 High-resolution spectra of N 1s of Al-MIL-53-NO$_2$ before (a) and after (b) being treated with 1.0 mM H$_2$S.
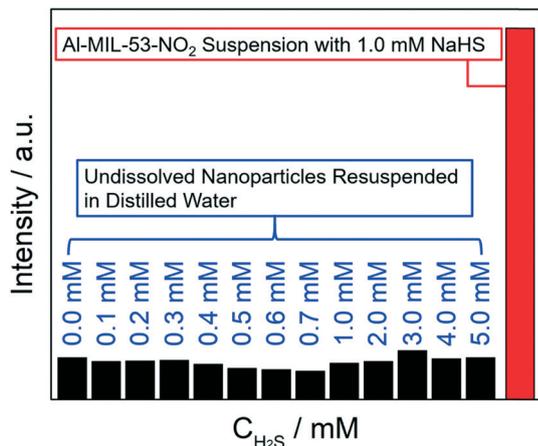
undissolved Al-MIL-53-NO$_2$ nanoparticles dispersed in water showed no fluorescence intensity and stayed in the "turn-off" mode (Fig. 5), which further confirmed that there were no –NH$_2$ groups at the surface of the undissolved H$_2$S-treated Al-MIL-53-NO$_2$ nanoparticles.

Overall, the recollected particles from H$_2$S treatment suspension were analyzed by XRD, SEM, FT-IR, PL, and XPS, and these nanoparticles were proved to be almost identical to the unreacted Al-MIL-53-NO$_2$ (0.1–1.0 mM). In addition, there were no –NH$_2$ groups attached to these remaining Al-MIL-53-NO$_2$ based on the FT-IR and XPS data, indicating that –NO$_2$ on the surface of Al-MIL-53-NO$_2$ were not converted to –NH$_2$. Therefore, it can be concluded that these remaining unreacted suspended Al-MIL-53-NO$_2$ particles made no contribution to the fluorescence enhancement in the H$_2$S sensing process.

3.3.2 Supernatant analysis. Since the fluorescence enhancement in the initial suspension system does not come from the undissolved Al-MIL-53-NO$_2$ nanoparticles treated with H$_2$S, the isolated supernatants were used for further analysis. The photoluminescence properties of the isolated supernatants were measured and the fluorescence enhancement was also observed under the supernatant system (Fig. 6(a–c)). It is interesting to find that a good linear relationship was also obtained upto 0.7 mM and the LOD of H$_2$S detection with the supernatant was calculated to be 69.7 μM (Fig. 6d, S2†), which indicated that the supernatant can be used to realize quantitative H$_2$S sensing as well.

To analyze the fluorophores in the supernatant, the transparent supernatant from 1.0 mM H$_2$S treated Al-MIL-53-NO$_2$ suspension was heated at 120 °C in air to evaporate the solvent and the extracts were characterized by FT-IR. Sodium

Fig. 5 Emission intensities at 450 nm (excitation wavelength: 339 nm) of aqueous solutions of undissolved nanoparticles (treated with 0.0 mM to 5.0 mM H_2S) (black columns) and Al-MIL-53-NO_2 suspension with 1.0 mM NaHS (red column).

2-aminoterephthalate, which serves as the real fluorophore in the solution, was detected in the FT-IR spectrum of the residues (Fig. S7†).[48] The broad peak with a maximum at 3370 cm^{-1} can be assigned to the amino groups interacting with the metal sodium after evaporation.[48,49] The completely deprotonated asymmetric and symmetric COO$^-$ vibrations were observed at 1590 cm^{-1} and 1371 cm^{-1}, respectively.[48]

Moreover, a very small amount of –NO_2 groups was also detected, indicating that BDC-NO_2 from Al-MIL-53-NO_2 existed in the supernatant after 1.0 mM H_2S treatment (Fig. S7†). Considering that no –NH_2 groups were observed on the undissolved Al-MIL-53-NO_2 nanoparticles (section 3.3.1), these results suggest that the linker BDC-NO_2 was first released because of Al-MIL-53-NO_2 degradation in the solution and then reduced to BDC-NH_2 by H_2S treatment. Such partial structural decomposition of the initial Al-MIL-53-NO_2 (Al–(OOC–NO_2^-) → Al–OH^- + NO_2–COO$^-$ (BDC-NO_2)) could stem from the replacement of the linkers by hydroxide ions (OH^-), which competitively bind to metal cations from the MOF clusters in the basic NaHS solution.[45,50] The conversion of –NO_2 to –NH_2 that occurs in the solution rather than on the MOF is probably because free BDC-NO_2 in the aqueous solution is more easily reduced by NaHS while the center of the Al–O clusters in solid-state Al-MIL-53-NO_2 increase the resistance towards NaHS attack. Therefore, it can be concluded that after H_2S treatment, a part of Al-MIL-53-NO_2 collapsed and the released BDC-NO_2 was reduced to BDC-NH_2, which gave rise to the fluorescence "turn-on" effect (Scheme 2).

The results of the above supernatant analysis matched well with the peak broadening in the XRD pattern, as discussed in the previous section (section 3.3.1). The remaining particles with reduced crystal size and the released fluorophores in the solution could also have an effect on the fluorescence signal. It is noteworthy that, for Al-MIL-53-NO_2
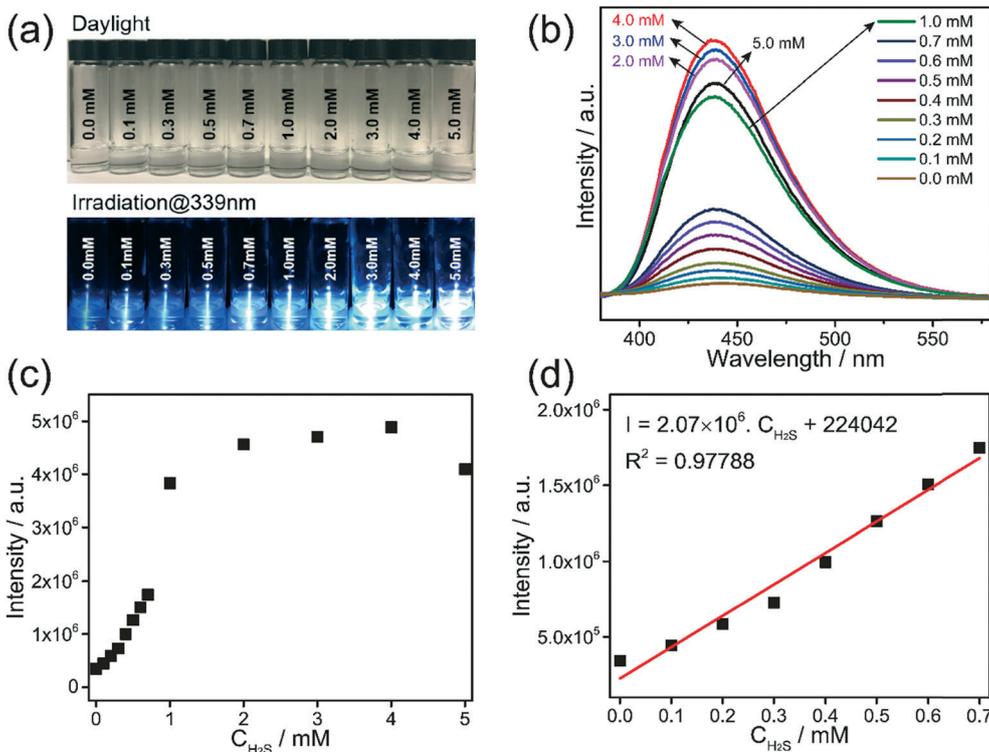
Fig. 6 (a) Digital images of Al-MIL-53-NO_2 supernatants separated from Al-MIL-53-NO_2 suspensions with various NaHS concentrations under visible light (up) and UV light (339 nm, down); (b) emission spectra of Al-MIL-53-NO_2 supernatants from Al-MIL-53-NO_2 supernatants with various NaHS concentrations (excitation wavelength: 339 nm); (c and d) emission intensity *versus* NaHS concentration.
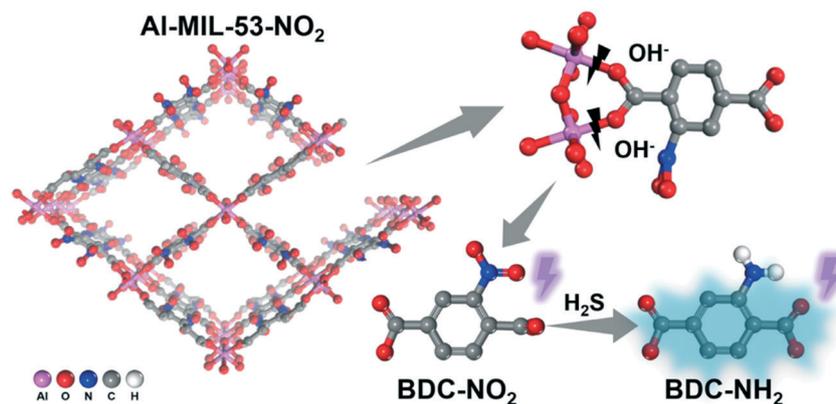
Scheme 2 Schematic illustration of Al-MIL-53-NO$_2$ in H$_2$S sensing.

treated with 1.0 mM H$_2$S, a much greater fluorescence intensity at 450 nm of the supernatant was achieved, as compared to that of the suspension (Fig. 7a). Such an enhancement in the emission of the supernatants can be also observed for Al-MIL-53-NO$_2$ upon treatment with H$_2$S at other concentrations (Fig. S8†). The reduced fluorescence of the suspension, as compared to the supernatant, is mainly caused by the unreacted non-luminescent Al-MIL-53-NO$_2$ dispersed in the aqueous system. The unreacted Al-MIL-53-NO$_2$ would absorb and scatter the incident excitation light and hence, decrease the photoluminescence intensity.[51] To further understand the emission difference between the supernatant and the suspension, we define relative reduction (η) as the ratio of fluorescence intensity difference between the supernatant and the suspension to that of the suspension,

$$\eta = \frac{I_{sup} - I_{sus}}{I_{sus}}$$

where I_{sup} is the fluorescence intensity of the suspension and I_{sup} is the fluorescence intensity of the supernatant (Fig. 7a). As shown in Fig. 7b, η increased from 2.25 at 0.1 mM (H$_2$S)

and reached the maximum value of 3.64 at 0.7 mM (H$_2$S), and then decreased with further increment of H$_2$S concentration until the minimum value of 0.15 was obtained at 5.0 mM. Such variations in the relative reduction (η) could be explained by the consumption of Al-MIL-53-NO$_2$ in the H$_2$S sensing process. When the H$_2$S concentration was less than 0.7 mM, only a small amount of Al-MIL-53-NO$_2$ was consumed, so the scattering effect of the remaining Al-MIL-53-NO$_2$ in the suspension system (0.1–0.7 mM) was almost the same. Therefore, with more interaction with H$_2$S (0.1–0.7 mM), more corresponding reaction product BDC-NH$_2$ was released into the solution and the linear relationship was maintained from 0.1 mM to 0.7 mM (Fig. 2c), considering that the scattering could be ignored. When Al-MIL-53-NO$_2$ was exposed to 1.0 mM H$_2$S, more initial Al-MIL-53-NO$_2$ collapsed and the scattering effect weakened sharply, so a much larger fluorescence enhancement in the suspension system was obtained and the linear relationship between the fluorescence intensity and H$_2$S concentration could not be maintained (Fig. 2c). This "turning point" was also reflected in the sharp reduction in η from 3.64 at 0.7 mM to 2.36 at 1.0
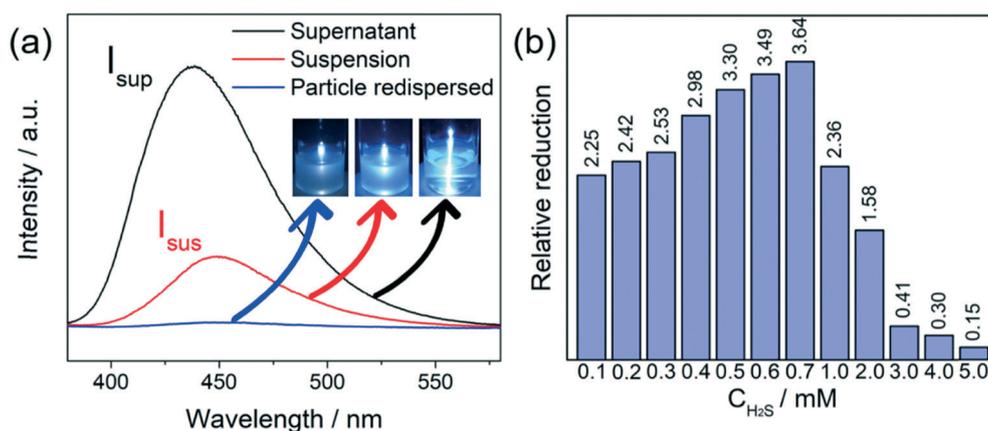
Fig. 7 (a) Emission spectra (monitored at 339 nm) of Al-MIL-53-NO$_2$ suspended in 1.0 mM NaHS solution (black line), Al-MIL-53-NO$_2$ supernatant separated from 1.0 mM NaHS treated Al-MIL-53-NO$_2$ suspension (red line), undissolved particles separated from 1.0 mM NaHS treated Al-MIL-53-NO$_2$ suspension re-dispersed in aqueous solution (blue line); (b) the relative reduction in the fluorescence intensity of Al-MIL-53-NO$_2$ treated with various NaHS concentrations.

mM (Fig. 7b). For 2.0–5.0 mM H_2S treatment suspensions, the initial Al-MIL-53-NO_2 was completely destroyed and the corresponding suspensions became more transparent (Fig. 2a), indicating that the scattering effect in this range could be neglected. Therefore, η tends to be stable and extremely small after being exposed to 2.0–5.0 mM H_2S (Fig. 7b).

4. Conclusion

In summary, the photoluminescence properties of Al-MIL-53-NO_2 for H_2S sensing have been systematically analyzed in both the suspension and the supernatant system. The mechanism of Al-MIL-53-NO_2 probe for H_2S detection unraveled that the fluorescence enhancement was ascribed to BDC-NH_2 reduction from BDC-NO_2 with the collapse of Al-MIL-53-NO_2 on exposure to H_2S. The undissolved nanoparticles treated with 0.1–1.0 mM H_2S were proved to be Al-MIL-53-NO_2 rather than Al-MIL-53-NH_2 with XRD, FT-IR, and XPS measurements, and these non-luminescence nanoparticles make no contribution to fluorescence enhancement in the "turn-on" process. In particular, both the suspension (LOD = 69.3 μM) and the supernatant (LOD = 69.7 μM) can be used for quantitative H_2S detection within 0–0.7 mM. This work provides a new insight into the ways of fluorophore location exploration in probe-consuming sensing applications.

Conflicts of interest

There are no conflicts to declare.

Acknowledgements

References

1 C. Szabó, *Nat. Rev. Drug Discovery*, 2007, **6**, 917.

2 G. Yang, L. Wu, B. Jiang, W. Yang, J. Qi, K. Cao, Q. Meng, A. K. Mustafa, W. Mu, S. Zhang, S. H. Snyder and R. Wang, *Science*, 2008, **322**, 587.

3 K. Eto, T. Asada, K. Arima, T. Makifuchi and H. Kimura, *Biochem. Biophys. Res. Commun.*, 2002, **293**, 1485–1488.

4 P. Kamoun, M.-C. Belardinelli, A. Chabli, K. Lallouchi and B. Chadefaux-Vekemans, *Am. J. Med. Genet., Part A*, 2003, **116A**, 310–311.

5 W. Yang, G. Yang, X. Jia, L. Wu and R. Wang, *J. Physiol.*, 2005, **569**, 519–531.

6 J. Polhemus David and J. Lefer David, *Circ. Res.*, 2014, **114**, 730–737.

7 W. Zhao, J. Zhang, Y. Lu and R. Wang, *EMBO J.*, 2001, **20**, 6008.

8 T. Amou, D. Hinode, M. Yoshioka and D. Grenier, *Int. J. Dent. Hyg.*, 2014, **12**, 145–151.

9 X. Liang, Y. He, F. Liu, B. Wang, T. Zhong, B. Quan and G. Lu, *Sens. Actuators, B*, 2007, **125**, 544–549.

10 M. T. S. R. Gomes, P. S. T. Nogueira and J. A. B. P. Oliveira, *Sens. Actuators, B*, 2000, **68**, 218–222.

11 C. Liu, J. Pan, S. Li, Y. Zhao, L. Y. Wu, C. E. Berkman, A. R. Whorton and M. Xian, *Angew. Chem., Int. Ed.*, 2011, **50**, 10327–10329.

12 F. Yu, X. Han and L. Chen, *Chem. Commun.*, 2014, **50**, 12234–12249.

13 G.-J. Mao, T.-T. Wei, X.-X. Wang, S.-y. Huan, D.-Q. Lu, J. Zhang, X.-B. Zhang, W. Tan, G.-L. Shen and R.-Q. Yu, *Anal. Chem.*, 2013, **85**, 7875–7881.

14 Y. Qian, J. Karpus, O. Kabil, S.-Y. Zhang, H.-L. Zhu, R. Banerjee, J. Zhao and C. He, *Nat. Commun.*, 2011, **2**, 495.

15 S. K. Bae, C. H. Heo, D. J. Choi, D. Sen, E.-H. Joe, B. R. Cho and H. M. Kim, *J. Am. Chem. Soc.*, 2013, **135**, 9915–9923.

16 O. M. Yaghi, M. O'Keeffe, N. W. Ockwig, H. K. Chae, M. Eddaoudi and J. Kim, *Nature*, 2003, **423**, 705–714.

17 T. Tian, Z. Zeng, D. Vulpe, M. E. Casco, G. Divitini, P. A. Midgley, J. Silvestre-Albero, J.-C. Tan, P. Z. Moghadam and D. Fairen-Jimenez, *Nat. Mater.*, 2017, **17**, 174.

18 H. Wang, X. Dong, E. Velasco, D. H. Olson, Y. Han and J. Li, *Energy Environ. Sci.*, 2018, **11**, 1226–1231.

19 X.-Y. Xu, X. Lian, J.-N. Hao, C. Zhang and B. Yan, *Adv. Mater.*, 2017, **29**, 1702298.

20 I. Abánades Lázaro and R. S. Forgan, *Coord. Chem. Rev.*, 2019, **380**, 230–259.

21 S. S. Nagarkar, T. Saha, A. V. Desai, P. Talukdar and S. K. Ghosh, *Sci. Rep.*, 2014, **4**, 7053.

22 S. S. Nagarkar, A. V. Desai and S. K. Ghosh, *Chem. – Eur. J.*, 2015, **21**, 9994–9997.

23 A. Buragohain and S. Biswas, *CrystEngComm*, 2016, **18**, 4374–4381.

24 X. Zhang, Q. Hu, T. Xia, J. Zhang, Y. Yang, Y. Cui, B. Chen and G. Qian, *ACS Appl. Mater. Interfaces*, 2016, **8**, 32259–32265.

25 Y.-Y. Cao, X.-F. Guo and H. Wang, *Sens. Actuators, B*, 2017, **243**, 8–13.

26 R. Dalapati, S. N. Balaji, V. Trivedi, L. Khamari and S. Biswas, *Sens. Actuators, B*, 2017, **245**, 1039–1049.

27 Y. Li, X. Zhang, L. Zhang, K. Jiang, Y. Cui, Y. Yang and G. Qian, *J. Solid State Chem.*, 2017, **255**, 97–101.

28 S. Nandi, H. Reinsch, S. Banesh, N. Stock, V. Trivedi and S. Biswas, *Dalton Trans.*, 2017, **46**, 12856–12864.

29 X. Zheng, R. Fan, Y. Song, A. Wang, K. Xing, X. Du, P. Wang and Y. Yang, *J. Mater. Chem. C*, 2017, **5**, 9943–9951.

30 Q. Gao, S. Xu, C. Guo, Y. Chen and L. Wang, *ACS Appl. Mater. Interfaces*, 2018, **10**, 16059–16065.

31 G. Lin, W. Meng and C. Dapeng, *Small*, 2018, **14**, 1703822.

32 S. Nandi, S. Banesh, V. Trivedi and S. Biswas, *Analyst*, 2018, **143**, 1482–1491.

33 H. Wang, J. Cui, A. Arshad, S. Xu and L. Wang, *Sci. China: Chem.*, 2018, **61**, 368–374.

34 Y. Zhan, L. Shen, C. Xu, W. Zhao, Y. Cao and L. Jiang, *CrystEngComm*, 2018, **20**, 3449–3454.

35 X. Zhang, Q. Zhang, D. Yue, J. Zhang, J. Wang, B. Li, Y. Yang, Y. Cui and G. Qian, *Small*, 2018, **14**, 1801563.

36 X. Zheng, R. Fan, Y. Song, K. Xing, P. Wang and Y. Yang, *ACS Appl. Mater. Interfaces*, 2018, **10**, 32698–32706.

37 X. Zhang, L. Fang, K. Jiang, H. He, Y. Yang, Y. Cui, B. Li and G. Qian, *Biosens. Bioelectron.*, 2019, **130**, 65–72.

38 D. Zhang, Y. Guan, E. J. M. Hensen, T. Xue and Y. Wang, *Catal. Sci. Technol.*, 2014, **4**, 795–802.

39 S. Biswas, T. Ahnfeldt and N. Stock, *Inorg. Chem.*, 2011, **50**, 9518–9526.

40 A. S. Munn, R. S. Pillai, S. Biswas, N. Stock, G. Maurin and R. I. Walton, *Dalton Trans.*, 2016, **45**, 4162–4168.

41 K. S. Walton and R. Q. Snurr, *J. Am. Chem. Soc.*, 2007, **129**, 8552–8556.

42 T. Xu, Z. Jiang, M. He, X. Gao and Y. He, *CrystEngComm*, 2019, **21**, 4820–4827.

43 S. Li, J. Wu, X. Gao, M. He, Y. Wang, X. Wang and Y. He, *CrystEngComm*, 2018, **20**, 7178–7183.

44 X. He and W.-N. Wang, *Dalton Trans.*, 2019, **48**, 1006–1016.

45 S. Yuan, L. Feng, K. Wang, J. Pang, M. Bosch, C. Lollar, Y. Sun, J. Qin, X. Yang, P. Zhang, Q. Wang, L. Zou, Y. Zhang, L. Zhang, Y. Fang, J. Li and H.-C. Zhou, *Adv. Mater.*, 2018, **30**, 1704303.

46 W. Li, M. Li, Y. Liu, D. Pan, Z. Li, L. Wang and M. Wu, *ACS Appl. Nano Mater.*, 2018, **1**, 1623–1630.

47 X.-X. Zheng, L.-J. Shen, X.-P. Chen, X.-H. Zheng, C.-T. Au and L.-L. Jiang, *Inorg. Chem.*, 2018, **57**, 10081–10089.

48 J. Sienkiewicz-Gromiuk, L. Mazur, A. Bartyzel and Z. Rzączyńska, *J. Inorg. Organomet. Polym. Mater.*, 2012, **22**, 1325–1331.

49 G. F. Oliveira, R. C. Andrade, A. B. Fortunato, E. S. Camargo and C. T. De Carvalho, *Brazilian Journal of Thermal Analysis*, 2015, **4**, 01–06.

50 X. Qian, B. Yadian, R. Wu, Y. Long, K. Zhou, B. Zhu and Y. Huang, *Int. J. Hydrogen Energy*, 2013, **38**, 16710–16715.

51 A. P. Demchenko, *Introduction to Fluorescence Sensing*, Springer, New York, 2015.